Cell

Ferroptosis: An Iron-Dependent Form of Nonapoptotic Cell Death

Scott J. Dixon,[1] Kathryn M. Lemberg,[1] Michael R. Lamprecht,[3] Rachid Skouta,[1] Eleina M. Zaitsev,[1] Caroline E. Gleason,[1] Darpan N. Patel,[1] Andras J. Bauer,[1] Alexandra M. Cantley,[1] Wan Seok Yang,[1] Barclay Morrison III,[3] and Brent R. Stockwell[1,2,4,*]

[1]Department of Biological Sciences
[2]Department of Chemistry
[3]Department of Biomedical Engineering
[4]Howard Hughes Medical Institute
Columbia University, 550 West 120th Street, Northwest Corner Building, MC 4846, New York, NY 10027, USA
*Correspondence: bstockwell@columbia.edu
DOI 10.1016/j.cell.2012.03.042

SUMMARY

Nonapoptotic forms of cell death may facilitate the selective elimination of some tumor cells or be activated in specific pathological states. The oncogenic RAS-selective lethal small molecule erastin triggers a unique iron-dependent form of nonapoptotic cell death that we term *ferroptosis*. Ferroptosis is dependent upon intracellular iron, but not other metals, and is morphologically, biochemically, and genetically distinct from apoptosis, necrosis, and autophagy. We identify the small molecule ferrostatin-1 as a potent inhibitor of ferroptosis in cancer cells and glutamate-induced cell death in organotypic rat brain slices, suggesting similarities between these two processes. Indeed, erastin, like glutamate, inhibits cystine uptake by the cystine/glutamate antiporter (system x_c^-), creating a void in the antioxidant defenses of the cell and ultimately leading to iron-dependent, oxidative death. Thus, activation of ferroptosis results in the nonapoptotic destruction of certain cancer cells, whereas inhibition of this process may protect organisms from neurodegeneration.

INTRODUCTION

Cell death is crucial for normal development, homeostasis, and the prevention of hyperproliferative diseases such as cancer (Fuchs and Steller, 2011; Thompson, 1995). It was once thought that almost all regulated cell death in mammalian cells resulted from the activation of caspase-dependent apoptosis (Fuchs and Steller, 2011; Thompson, 1995). More recently, this view has been challenged by the discovery of several regulated nonapoptotic cell death pathways activated in specific disease states, including poly(ADP-ribose) polymerase-1 (PARP-1) and apoptosis-inducing factor 1 (AIF1)-dependent parthanatos, caspase-1-dependent pyroptosis, and receptor-interacting protein kinase 1 (RIPK1)-dependent necroptosis (Bergsbaken et al., 2009; Christofferson and Yuan, 2010; Wang et al., 2009). We hypothesized that additional regulated forms of nonapoptotic cell death likely remain to be discovered that mediate cell death in other developmental or pathological circumstances.

The RAS family of small GTPases (HRAS, NRAS, and KRAS) are mutated in ~30% of all cancers (Vigil et al., 2010). Finding compounds that are selectively lethal to RAS mutant tumor cells is therefore a high priority. We previously identified two structurally unrelated small molecules, named erastin and RSL3, that were selectively lethal to oncogenic RAS mutant cell lines and that we refer to together as RAS-selective lethal (RSL) compounds (Dolma et al., 2003; Yang and Stockwell, 2008). Using affinity purification, we identified voltage-dependent anion channels 2 and 3 (VDAC2/3) as direct targets of erastin (Yagoda et al., 2007), but not RSL3. Short hairpin RNA (shRNA) and complementary DNA (cDNA) overexpression studies demonstrated that VDAC2 and VDAC3 are necessary, but not sufficient, for erastin-induced death (Yagoda et al., 2007), indicating that additional unknown targets are required for this process.

The type of cell death activated by the RSLs has been enigmatic. Classic features of apoptosis, such as mitochondrial cytochrome c release, caspase activation, and chromatin fragmentation, are not observed in RSL-treated cells (Dolma et al., 2003; Yagoda et al., 2007; Yang and Stockwell, 2008). RSL-induced death is, however, associated with increased levels of intracellular reactive oxygen species (ROS) and is prevented by iron chelation or genetic inhibition of cellular iron uptake (Yagoda et al., 2007; Yang and Stockwell, 2008). In a recent systematic study of various mechanistically unique lethal compounds, the prevention of cell death by iron chelation was a rare phenomenon (Wolpaw et al., 2011), suggesting that few triggers can access iron-dependent lethal mechanisms.

We have explored the hypothesis that RSLs such as erastin activate a lethal pathway that is different from apoptosis, necrosis, and other well-characterized types of regulated cell death. We find that erastin-induced death involves a unique constellation of morphological, biochemical, and genetic features, which led us to propose the name *ferroptosis* as a description for this phenotype. We identified a specific

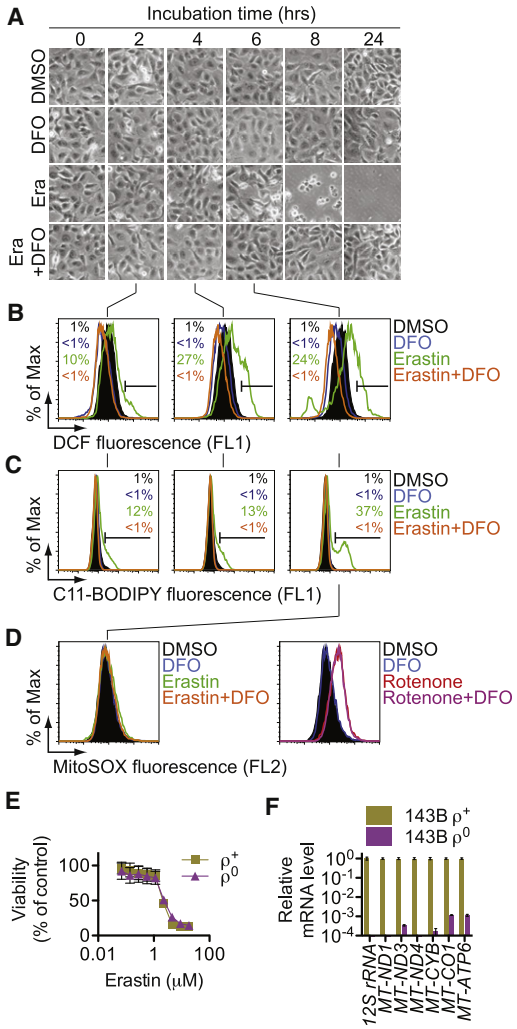

Figure 1. Erastin-Induced Death Triggers the Accumulation of Cytosolic ROS, Whose Production Can Be Inhibited by DFO

(A) Visualization of HT-1080 cell viability over time ±erastin (Era, 10 μM) and deferoxamine (DFO, 100 μM).

(B and C) Cytosolic and lipid ROS production assessed over time (2, 4, and 6 hr) by flow cytometry using H_2DCFDA and C11-BODIPY.

(D) Mitochondrial ROS assessed in HT-1080 cells treated for 6 hr with erastin ±DFO, as above, or with rotenone (250 nM) ±DFO. In (A)–(D), representative data from one of four experiments are shown.

(E) Erastin-induced death in 143B ρ^0 and ρ^+ cells.

(F) mtDNA-encoded transcript levels in ρ^0 and ρ^+ cells. Results in (E) and (F) are mean ±SD from one of three representative experiments.

See Figure S1 for additional data showing that iron-dependent cell death occurs independently of the mitochondrial electron transport chain.

small-molecule inhibitor of ferroptosis (ferrostatin-1) that prevents ferroptosis in cancer cells, as well as glutamate-induced cell death in postnatal rat brain slices. Our results suggest an underlying similarity between diverse forms of iron-dependent, nonapoptotic death and that the manipulation of ferroptosis may be exploited to selectively destroy RAS mutant tumor cells or to preserve neuronal cells exposed to specific oxidative conditions.

RESULTS

Erastin Triggers Oxidative, Iron-Dependent Cell Death

RSL-induced cell death is a poorly characterized process involving the accumulation of ROS derived from an unknown source and the inhibition of cell death by iron chelation (Yagoda et al., 2007; Yang and Stockwell, 2008). We observed that these two processes were linked. Treatment of *NRAS* mutant HT-1080 fibrosarcoma cells with the RSL molecule erastin (10 μM) resulted in a time-dependent increase in cytosolic and lipid ROS beginning at 2 hr, as assayed by flow cytometry using the fluorescent probes H_2DCFDA and C11-BODIPY, respectively (Figures 1B and 1C). This increase in ROS preceded cell detachment and overt death, which began at 6 hr (Figure 1A). ROS accumulation and cell death were suppressed by cotreatment with the iron chelator deferoxamine (DFO, 100 μM) (Figures 1A–1C), whereas incubation with three different exogenous sources of iron, but not with other divalent transition metal ions (Cu^{2+}, Mn^{2+}, Ni^{2+}, and Co^{2+}), potentiated erastin-induced death (Figures S1A and S1B available online). As cell death occurred in erastin-treated cells following a prolonged period of ROS accumulation and was suppressed by antioxidants (see below), our data suggest that the overwhelming, iron-dependent accumulation of ROS is what kills these cells.

Because two erastin targets, VDAC2 and VDAC3, reside in the mitochondria, we hypothesized that erastin-induced death involved aberrant ROS production by the mitochondrial electron transport chain (ETC). However, in erastin-treated (10 μM, 6 hr) HT-1080 cells, we observed no increase in MitoSOX-sensitive mitochondrial ROS production (Figure 1D, left). The ETC complex I inhibitor rotenone (250 nM, 6 hr) enhanced MitoSOX-sensitive ROS production but in a manner that was insensitive to DFO (Figure 1D, right). Furthermore, *KRAS* mutant 143B osteosarcoma cells incapable of ETC-dependent ROS formation, due to the depletion of mitochondrial DNA (mtDNA)-encoded transcripts (ρ^0 cells), were as sensitive to erastin and RSL3 as matched mtDNA-wild-type (ρ^+) cells (Figures 1E, 1F, and S1C–S1E). Thus, erastin-induced cell death in human cancer cells involves DFO-sensitive ROS accumulation and can occur in cells lacking a functional mitochondrial ETC.

Ferroptosis Is Distinct from Known Forms of Cell Death

We examined whether ferroptosis shared morphological, bioenergetic, or other similarities with apoptotic or necrotic death or with autophagy. Using transmission electron microscopy, we observed that *HRAS* mutant BJeLR-engineered tumor cells treated with erastin exhibited none of the characteristic morphologic features associated with staurosporine (STS)-induced apoptosis (e.g., chromatin condensation and margination), hydrogen peroxide (H_2O_2)-induced necrosis (e.g., cytoplasmic and organelle swelling, plasma membrane rupture), or rapamycin-induced autophagy (e.g., formation of double-membrane enclosed vesicles) (Figure 2A). The lone distinctive morphological feature of erastin-treated cells involved mitochondria that appeared smaller than normal with increased membrane density, consistent with our previous report (Yagoda et al., 2007) (Figure 2A). With respect to bioenergetics, we observed substantial depletion of intracellular ATP in BJeLR and HT-1080 cells treated

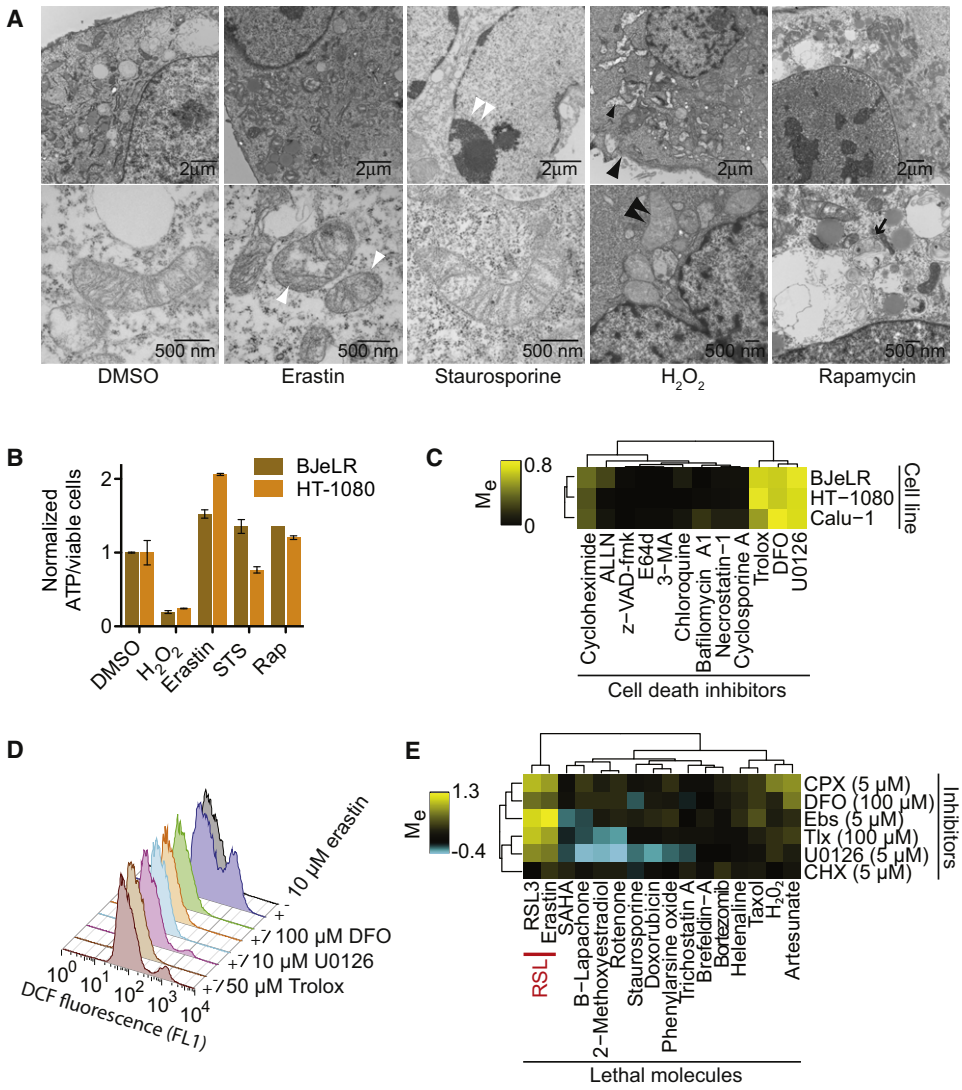

Figure 2. Erastin-Induced Oxidative Death Is Iron Dependent

(A) Transmission electron microscopy of BJeLR cells treated with DMSO (10 hr), erastin (37 μM, 10 hr), staurosporine (STS, 0.75 μM, 8 hr), H_2O_2 (16 mM, 1 hr), and rapamycin (Rap, 100 nM, 24 hr). Single white arrowheads, shrunken mitochondria; paired white arrowheads, chromatin condensation; black arrowheads, cytoplasmic and organelle swelling and plasma membrane rupture; black arrow, formation of double-membrane vesicles. A minimum of 10 cells per treatment condition were examined.

(B) Normalized ATP levels in HT-1080 and BJeLR cells treated as in (A) with the indicated compounds. Representative data (mean ±SD) from one of three independent experiments are shown.

(C) Modulatory profiling of known small-molecule cell death inhibitors in HT-1080, BJeLR, and Calu-1 cells treated with erastin (10 μM, 24 hr).

(D) Effect of inhibitors on H_2DCFDA-sensitive ROS production in HT-1080 cells treated for 4 hr.

(E) Modulatory profiling of ciclopirox olamine (CPX), DFO, ebselen (Ebs), trolox (Tlx), U0126, and CHX on oxidative and nonoxidative lethal agents.

See Figure S2 for related data showing that iron-dependent cell death is independent of proapoptotic proteins.

with H_2O_2, but not erastin, STS, or rapamycin (Figure 2B), distinguishing ferroptosis from various forms of necrosis that involve bioenergetic failure.

Using a variation of our recently reported modulatory profiling strategy (Wolpaw et al., 2011), we tested the ability of 12 established small-molecule cell death inhibitors to prevent ferroptosis in HT-1080 cells, BJeLR cells, and *KRAS* mutant Calu-1 non-small cell lung cancer cells. We computed the modulatory effect (M_e) for each inhibitor (tested in a 10 point, 4-fold dilution series) on the normalized viability of cells treated with a lethal dose of erastin ($M_e < 0$, death sensitization; $M_e = 0$, no effect; $M_e > 0$, death rescue). The resulting values were clustered hierarchically in an unsupervised fashion and displayed as a heat map. Using this approach, we observed that erastin-induced death was not consistently modulated by inhibitors of caspase, cathepsin, or calpain proteases (z-VAD-fmk, E64d, or ALLN); RIPK1 (necrostatin-1); cyclophilin D (cyclosporin A); or lysosomal function/autophagy (bafilomycin A1, 3-methyladenine, chloroquine),

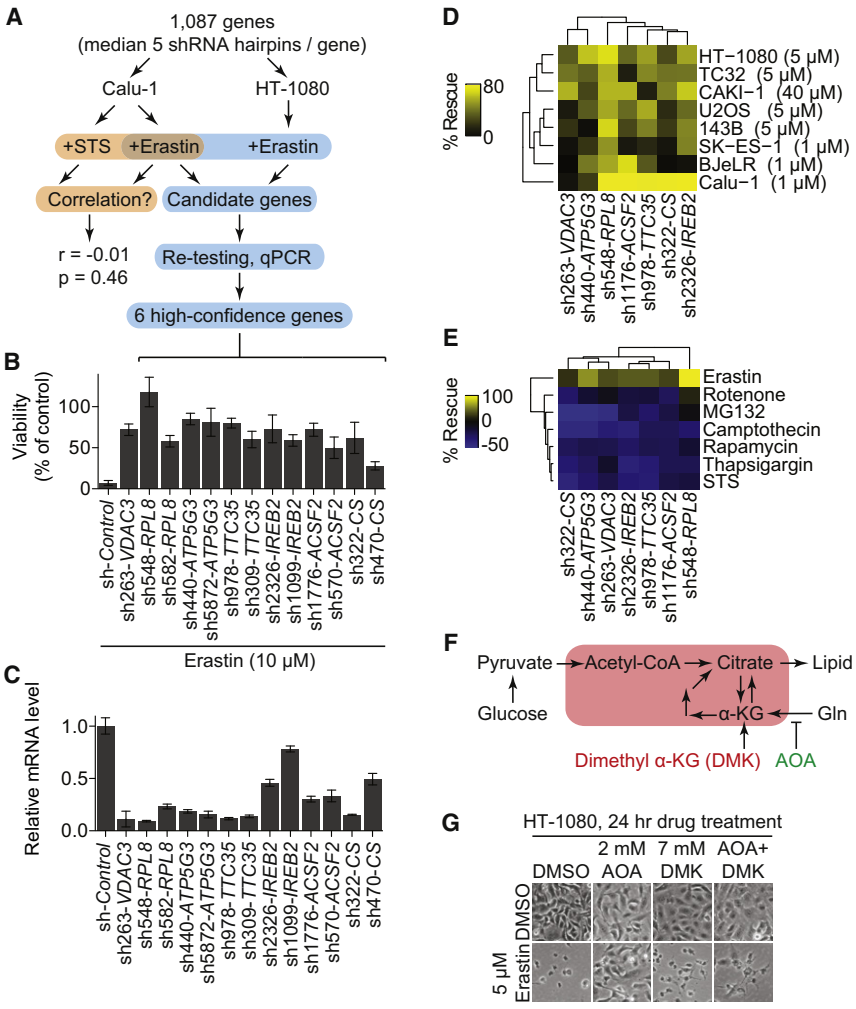

Figure 3. Erastin-Induced Ferroptosis Exhibits a Unique Genetic Profile

(A) Outline of the shRNA screen and confirmation pipeline.

(B and C) Six high-confidence genes required for erastin-induced ferroptosis. (B) Viability of HT-1080 cells infected with shRNAs for 72 hr and treated with erastin (10 μM, 24 hr). (C) mRNA levels for hairpins shown in (B) determined by using RT-qPCR. Data in (B) and (C) are mean ±SD from one of three experiments.

(D and E) Effect of shRNA-mediated silencing of high-confidence genes by using the best hairpin identified by mRNA silencing efficiency in (C) on cell viability. (D) Viability of various cell lines treated with a lethal dose of erastin (indicated in brackets) for 24 hr. (E) Viability of HT-1080 cells treated with various death-inducing or cytostatic compounds. For (D) and (E), % rescue was computed relative to each shRNA alone +DMSO.

(F) Cartoon outline of glutamine (Gln) metabolism. Red box indicates mitochondria.

(G) Images of HT-1080 cells treated with amino-oxyacetic acid (AOA) ±dimethyl α-ketoglutarate (DMK) ±erastin.

See also Figure S3.

which are compounds known to inhibit forms of apoptosis, necrosis, and autophagic cell death (Figure 2C).

DFO, the antioxidant trolox, the MEK inhibitor U0126, and, to a weaker extent, the protein synthesis inhibitor cycloheximide (CHX), all rescued from erastin-induced death in HT-1080, BJeLR, and Calu-1 cells (Figure 2C) (Yagoda et al., 2007). These inhibitors were also effective at preventing erastin-induced ferroptosis in both wild-type and apoptosis-deficient *Bax*/*Bak* double knockout (DKO) mouse embryonic fibroblasts (Figures S2A and 2B), indicating that ferroptosis can be activated in human-derived and mouse-derived cells and is independent of the core apoptotic machinery regulated by *Bax* and *Bak*. DFO, trolox, and U0126 all prevented the accumulation of H_2 DCFDA-sensitive ROS in erastin-treated HT-1080 cells (Figure 2D), demonstrating that these inhibitors act to prevent death upstream or at the level of ROS production. Because trolox, U0126, and the membrane-permeable iron chelator 2,2-bipyridyl could be added to HT-1080 cells up to 6 hr after erastin and still confer substantial protection from death (Figure S2C), ferroptosis likely requires continuous iron-dependent ROS formation over an extended period of time to trigger death.

Finally, in a modulatory profiling experiment that tested the ability of DFO, trolox, U0126, CHX, the membrane-permeable iron chelator ciclopirox olamine (CPX), and the glutathione peroxidase mimetic ebselen (Ebs) to modulate the lethality of erastin, RSL3, or 16 other mechanistically distinct lethal compounds thought to kill cells through various ROS-dependent and ROS-independent mechanisms, we observed that erastin and RSL3 formed a distinct cluster that was separate from all other inducers of cell death (Figure 2E). Together, these data support the hypothesis that RSL-induced ferroptosis is distinct from apoptosis, various forms of necrosis, and autophagy.

Ferroptosis Is Regulated by a Distinct Set of Genes

To explore the genetic basis of ferroptosis, we sought to identify genes uniquely required for this process. We focused on the potential role of the mitochondria, as this organelle displayed an aberrant morphology in erastin-treated cells (Figure 2A). Mitochondrial gene function was perturbed using a custom arrayed-shRNA library targeting 1,087 genes (median 5 hairpins/gene), most of which (901, 88%) encode predicted mitochondrial proteins (Pagliarini et al., 2008) (Figure 3A). Using this library, we first compared the genetic suppressibility of erastin (7.3 μM)-induced ferroptosis and STS (1 μM)-induced apoptosis in Calu-1 cells (Figure 3A). Across all 5,817 informative hairpins, we observed no significant correlation between those shRNAs that rescued from erastin-induced ferroptosis and those that rescued from STS-induced apoptosis (Spearman rank sum test, $r = -0.01$, $p = 0.46$), confirming that distinct genetic networks govern erastin-induced ferroptosis and STS-induced apoptosis.

Next, we performed a second erastin resistance screen in HT-1080 cells and, by using a rigorous confirmation pipeline, identified six high-confidence genes supported by at least two independent shRNAs per gene that are required for erastin-induced ferroptosis in both HT-1080 and Calu-1 cells: ribosomal protein L8 (*RPL8*), iron response element binding protein 2 (*IREB2*), ATP synthase F_0 complex subunit C3 (*ATP5G3*), citrate synthase (*CS*), tetratricopeptide repeat domain 35 (*TTC35*), and acyl-CoA synthetase family member 2 (*ACSF2*) (Figures 3B and 3C). Consistent with the established CHX- and DFO-sensitive nature of erastin-induced ferroptosis, *RPL8* encodes a component of the 60S ribosomal subunit presumably required for translation, and *IREB2* encodes a master regulator of iron metabolism. We further validated these results, showing that shRNA-mediated silencing of *IREB2* and the IREB2 negative regulator *FBXL5* (Salahudeen et al., 2009; Vashisht et al., 2009) resulted in reciprocal changes in the expression of the known iron uptake, metabolism, and storage genes *TFRC*, *ISCU*, *FTH1*, and *FTL* and in erastin sensitivity (Figures S3A–S3C). These results provide confidence in the quality of the screening and confirmation procedures.

To establish the generalizability of the results obtained in HT-1080 and Calu-1 cells, we tested the effects of silencing these genes in HT-1080, Calu-1, and six additional cell lines treated with erastin. Silencing of these six high-confidence genes by using the most effective hairpin for each gene, defined by mRNA silencing levels in HT-1080 cells (Figure 3C), conferred $\geq$20% rescue in 79% (38/48) of shRNA by cell line combinations (Figure 3D). Thus, these genes appear to be broadly required for erastin-induced ferroptosis. We next tested whether silencing of these genes specifically attenuated erastin-induced ferroptosis or more broadly modulated a variety of lethal effects. Silencing of these six genes conferred protection against erastin-induced ferroptosis ($\geq$40% rescue for 6/6 hairpins), but not cell death/cytostasis induced by STS, rotenone, rapamycin, the proteasome inhibitor MG132, the DNA-damaging agent camptothecin, or the Ca^{2+}-dependent ATPase inhibitor thapsigargin ($\geq$40% rescue for 0/6 hairpins) (Figure 3E). Together, these data support the hypothesis that a unique genetic network governs erastin-induced ferroptosis compared to other forms of cell death.

Both *ACSF2* and *CS* are implicated in the regulation of mitochondrial fatty acid metabolism (Mullen et al., 2011; Watkins et al., 2007), and we wondered whether this process could contribute to ferroptosis. In cancer cells, fatty acid synthesis is in part dependent upon the metabolism of glutamine (Gln) to α-ketoglutarate, a process that can be inhibited by the small-molecule transaminase inhibitor aminooxyacetic acid (AOA) (Wise et al., 2008) (Figure 3F). In cell culture media containing both glucose and Gln, we found that AOA (2 mM) rescued both HT-1080 and BJeLR cells from erastin-induced ferroptosis (Figures 3F and S3D), mimicking the effects of silencing *CS* and *ACSF2*. In AOA-treated HT-1080 cells, the lethality of erastin was restored by coincubation with dimethyl α-ketoglutarate (DMK), which provides the downstream metabolite whose production from Gln is blocked by AOA (Wise et al., 2008) (Figures 3F and 3G). Dichloroacetic acid (DCA), an unrelated modulator of mitochondrial function not predicted to directly affect Gln metabolism, had no effect on erastin-induced ferroptosis (Figure S3D). These results suggest that a Gln-, *CS*-, and *ACSF2*-dependent lipid synthesis pathway could supply a specific lipid precursor required for ferroptosis.

Identification of Ferrostatin-1 as a Small-Molecule Inhibitor of Ferroptosis

One ultimate aim is to investigate the potential role of ferroptosis in vivo, and we therefore sought to identify a potent and specific drug-like small-molecule inhibitor of this process. To overcome the inherent limitations of many individual small-molecule collections (Macarron et al., 2011), we assembled a custom screening library of 9,517 small molecules derived from a starting pool of 3,372,615 commercially available compounds that were filtered in silico on the basis of drug likeness, solubility, scaffold diversity, and other parameters. Screening of this lead-optimized compound (LOC) library and subsequent confirmation studies identified a compound that we named ferrostatin-1 (Fer-1) as the most potent inhibitor of erastin-induced ferroptosis in HT-1080 cells (EC_{50} = 60 nM) (Figures 4A, S4A, and S4B). To our knowledge, the activity for Fer-1 has not previously been reported in any biological system. We performed a total synthesis of Fer-1 (see Extended Experimental Procedures) and used this material to confirm the activity of Fer-1 and demonstrate that it specifically inhibited RSL-induced death, but not cell death induced by other oxidative lethal compounds and apoptosis-inducing agents (Figures 4B and 6A).

We next sought to define the Fer-1 mechanism of action. Fer-1 did not inhibit extracellular signal-regulated kinase (ERK) phosphorylation or arrest the proliferation of HT-1080 cells, suggesting that it does not inhibit the MEK/ERK pathway, chelate iron, or inhibit protein synthesis (Figures 4C and 4D). Fer-1 did, however, prevent erastin-induced accumulation of cytosolic and lipid ROS (Figure 4E). Moreover, similar to the positive control antioxidant trolox, Fer-1 readily oxidized the stable radical 2,2-diphenyl-1-picrylhydrazyl (DPPH) under cell-free conditions, a test of intrinsic antioxidant potential (Figure 4F). Substitution of the primary aromatic amine for a nitro group (SRS8-24) or elimination of the N-cyclohexyl moiety (CA-1) destroyed the antioxidant capability of Fer-1 as well as its ability to prevent erastin (10 μM)-induced death in HT-1080 cells (Figures 4F–4H). Thus, both aromatic amines are required for Fer-1 to prevent RSL-induced death, a function plausibly linked to its ability to scavenge free radicals.

Our results suggested that lipid ROS were crucial for erastin-induced death. We therefore hypothesized that Fer-1 was a lipid ROS scavenger, with the N-cyclohexyl moiety serving as a lipophilic anchor within biological membranes. Consistent with this hypothesis, in a series of ten Fer-1 analogs in which the number of carbons in the N-substituted cyclic moiety was systematically varied, we observed a significant correlation between the predicted lipophilicity (octanol-water partition coefficient, log P) and the erastin-death-suppressing ability of each molecule (Spearman R = -0.85, p = 0.002) (Figures 4I and S4C). Of note, SRS8-72, a Fer-1 analog with N-cyclopropyl in place of N-cyclohexyl, which was an order of magnitude less potent than Fer-1 at preventing death, nonetheless retained equivalent intrinsic antioxidant capability in the cell-free DPPH assay (Figures 4F–4H and S4C). Thus, the N-cyclohexyl moiety likely

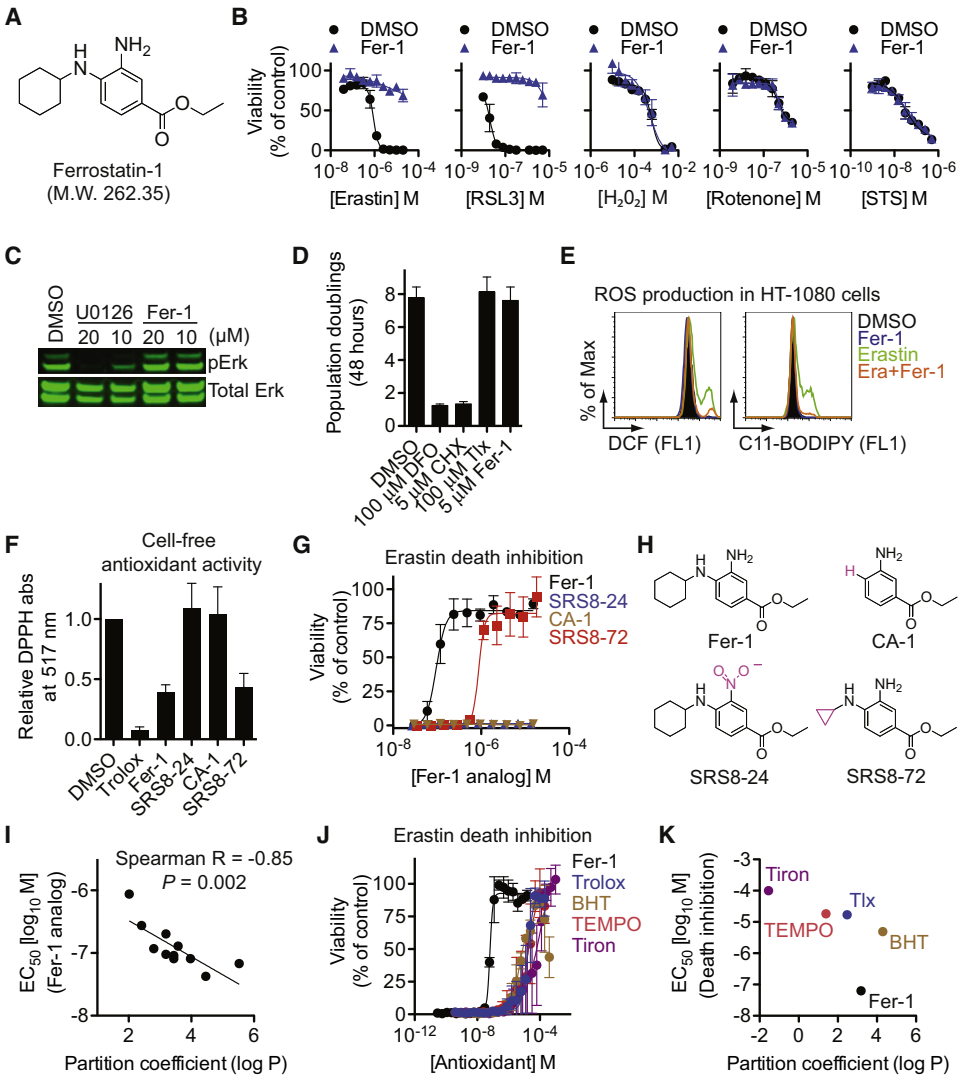

Figure 4. Identification and Characterization of Ferrostatin-1

(A) Structure of ferrostatin-1 (Fer-1). The molecular weight (MW) is indicated.

(B) Effect of resynthesized Fer-1 (0.5 μM) on the lethality of various compounds in HT-1080 cells. All drug treatments were for 24 hr.

(C) Effect of Fer-1 and U0126 on ERK phosphorylation in HT-1080 cells.

(D) Effect of DFO, CHX, trolox (Tlx), and Fer-1 on HT-1080 cell proliferation over 48 hr as assessed by Vi-Cell.

(E) Effect of Fer-1 (0.5 μM) on erastin (10 μM)-induced ROS production in HT-1080 cells (4 hr treatment).

(F) Cell-free antioxidant potential monitored by changes is the absorbance at 517 nm of the stable radical DPPH.

(G) Dose-response relationship for inhibition of erastin (10 μM, 24 hr)-induced death in HT-1080 cells by Fer-1 and analogs.

(H) Chemical structure of various Fer-1 analogs tested in (F) and (G).

(I) Correlation between predicted partition coefficient (log P) and the ability of various Fer-1 analogs to prevent erastin-induced death.

(J) Dose-response relationship for inhibition of erastin (10 μM, 24 hr)-induced death by various antioxidants.

(K) Plot of predicted partition coefficient (log P) and ability of various antioxidants to prevent erastin-induced death. Data in (B), (D), (F), (G), and (J) represent mean ±SD from one of three representative experiments.

For additional data on Fer-1 identification and characterization, see also Figure S4.

enables Fer-1 to prevent ferroptosis by promoting the tethering of Fer-1 within lipid membranes, as opposed to influencing the intrinsic antioxidant potential of this molecule.

Intriguingly, lipid partitioning alone does not appear to be sufficient to account for the potency of Fer-1. Fer-1 has similar predicted lipophilicity but much greater erastin-suppressing potency than two canonical lipophilic antioxidants (trolox and butylated hydroxyltoluene [BHT]) while being both considerably more lipophilic and more potent than two representative soluble antioxidants (Tiron and TEMPO) (Figures 4J and 4K). Both trolox and BHT are phenolic antioxidants, whereas Fer-1 contains an aromatic amine. We hypothesize that this difference may confer a unique profile of radical reactivity upon Fer-1 that is better tuned to the RSL mechanism.

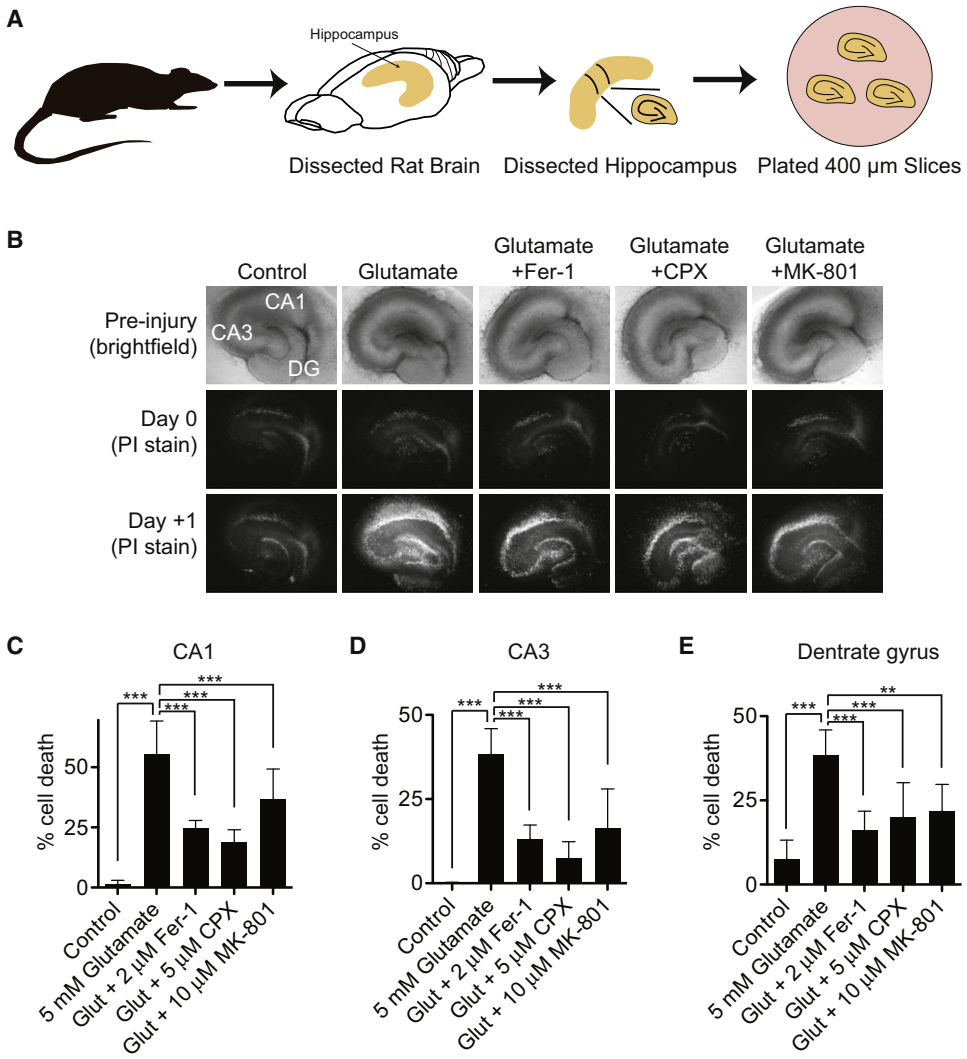

Figure 5. Effects of Fer-1 on Excitotoxic Cell Death in Organotypic Hippocampal Slice Cultures

(A) Cartoon outline of hippocampal slice procedure.

(B) Bright-field and fluorescent images of PI staining of treated hippocampal slices. Slices were treated with glutamate (5 mM, 3 hr) ±Fer-1 (2 μM), CPX (5 μM), or MK-801 (10 μM). Representative images from 1 of 6 slices per condition are shown.

(C–E) Quantification of the effects depicted in (B). Data shown are mean ±SD. Data were analyzed using a two-way ANOVA (brain region x drug treatment) followed by Bonferroni posttests.

**p < 0.01 and ***p < 0.001.

Fer-1 Prevents Glutamate-Induced Neurotoxicity

Excitotoxic cell death that occurs in the nervous system in epilepsy, stroke, and other trauma situations has been described as an oxidative, iron-dependent process (Cheah et al., 2006; Choi, 1988; Murphy et al., 1989). We hypothesized that excitotoxic death could be related to erastin-induced ferroptosis. We tested this hypothesis by using a rat organotypic hippocampal slice culture (OHSC) model that closely resembles the hippocampus in vivo by preserving the integrity of neuronal connections, both inhibitory and excitatory, and their supporting cells, including astrocytes and microglia (Lossi et al., 2009). OHSCs have proven to be ideal complex preparations for lead-compound identification and validation (Noraberg et al., 2005; Sundstrom et al., 2005), capable of predicting in vivo efficacy (Cater et al., 2007; Morrison et al., 2002).

OHSCs were treated with a lethal excitotoxic stimulus (5 mM L-glutamate, 3 hr) that mimics the consequences of stroke and neurodegenerative disease (Morrison et al., 2002; Sundstrom et al., 2005) (Figure 5A). These slices were coincubated with glutamate and vehicle alone or with glutamate plus Fer-1 (2 μM), the iron chelator CPX (5 μM), or, as a positive control, the *N*-methyl-D-aspartate (NMDA) receptor antagonist MK-801 (10 μM). We analyzed the effects of these compound treatments on propidium iodide (PI) uptake as an indicator of cell death 24 hr following the end of glutamate treatment in three defined regions of the OHSCs: the dentate gyrus (DG), the CA1, and the CA3

fields of the hippocampus. A two-way analysis of variance (ANOVA) suggested significant differences for both brain region ($F_{2,75} = 19.23$, $p < 0.0001$) and compound treatment ($F_{4,75} = 67.8$, $p < 0.0001$) factors. Focusing on the compound treatment effect, Bonferroni posttests indicated that glutamate induced significant cell death in all three regions of the brain and that this death was attenuated significantly and to an almost identical extent by cotreatment with Fer-1, CPX, or MK-801 ($p < 0.001$ for all interactions except glutamate+MK-801 within the DG, $p < 0.01$) (Figures 5B–5E). These results suggest that glutamate-induced death in OHSCs and erastin-induced death in cancer cells share in common a core lethal mechanism that can be inhibited by iron chelation or Fer-1.

Erastin Inhibits System x_c^-

CPX and Fer-1 suppressed erastin-induced death in cancer cells and glutamate-induced toxicity in OHSCs, consistent with a common iron- and ROS-dependent death execution mechanism. We wondered whether any death-initiating mechanisms could also be shared between these two processes.

Glutamate-induced death in brain cells can be initiated by calcium influx through ionotropic glutamate receptors and through competitive inhibition of cystine uptake by the Na^+-independent cystine/glutamate antiporter, system x_c^- (Choi, 1988; Murphy et al., 1989). The calcium chelators BAPTA-AM, Fura-2, and EGTA had no effect on erastin-induced death (Figure S5A) (Wolpaw et al., 2011), arguing against a role for Ca^{2+} influx in this process. However, we observed striking clustering of erastin and sulfasalazine (SAS), a specific inhibitor of system x_c^- (Gout et al., 2001), in a modulatory profile of 19 oxidative and nonoxidative lethal molecules generated in HT-1080 cells (Figure 6A). If blockade of system x_c^--mediated cystine import can trigger ferroptosis, then providing this metabolite to cells through an alternative means should rescue from death. Indeed, β-mercaptoethanol (β-ME), which can circumvent the inhibition of system x_c^- by promoting cystine uptake through an alternative pathway (Ishii et al., 1981), strongly inhibited cell death in HT-1080 cells induced by erastin, SAS, and glutamate (Figures 6A and S5B). As predicted by these results, SAS, like erastin, behaved as an RSL compound, albeit with considerably lower potency than erastin (Figure S5C). This is nonetheless noteworthy, as SAS is an FDA-approved drug not previously shown to demonstrate such activity.

System x_c^- is a disulfide-linked heterodimer composed of SLC7A11 (xCT) and SLC3A2 (4F2hc and CD98hc) (Sato et al., 1999) (Figure 6B). Inhibition of system x_c^- can lead to a compensatory transcriptional upregulation of *SLC7A11* (Lo et al., 2008). Consistent with this, we observed substantial upregulation of *SLC7A11* in HT-1080 cells that were treated with erastin or SAS, an effect that was suppressed by β-ME, but not DFO or Fer-1 (Figure 6C). Further confirming the relevance of system x_c^- to erastin-induced ferroptosis, siRNA-mediated silencing of *SLC7A11* with two independent siRNAs sensitized HT-1080 cells to erastin-induced death (Figures 6D and 6E), whereas transfection of HT-1080 cells with a plasmid encoding DDK-tagged *SLC7A11* conferred protection from erastin- and SAS-induced death (Figure S5D). Given these results, we directly examined the uptake of [^{14}C]-cystine into HT-1080 cells. Erastin (10 μM), glutamate (50 mM), and SAS (1 mM) abolished the Na^+-independent uptake of [^{14}C]-cystine, whereas RSL3 had no effect on this process (Figures 6F and S5E).

How does erastin inhibit system x_c^-? Analysis of affinity purification data (Yagoda et al., 2007) identified SLC7A5 (LAT1, 4F2lc, and CD98lc) as the lone protein bound by an active erastin affinity analog in lysates from both *HRAS*-wild-type BJeH and *HRAS* mutant BJeLR cells (Figure 6G). SLC7A5 (like SLC7A11) is one of six light chains that bind SLC3A2 to form amino acid transporters of differing substrate selectivity. The SLC7A5/SLC3A2 complex (system L) transports large, neutral amino acids (Kanai and Endou, 2003) (Figure 6B). In a profile of 123 metabolites from human Jurkat T lymphocytes treated with erastin (1 μM, 25 min) (Ramanathan and Schreiber, 2009), highly significant decreases were observed in the levels of system L substrates (Kanai and Endou, 2003), whereas the levels of nonsystem L substrates were unchanged or increased (Figure 6H). However, unlike inhibition of system x_c^- using excess glutamate (12.5 mM), inhibition of system L using excess D-phenylalanine (12.5 mM) (Kanai and Endou, 2003) did not strongly sensitize to erastin (Figure 6I). Together, this suggests that erastin inhibits system L-mediated amino acid uptake but that this does not contribute directly to ferroptosis. Rather, erastin binding to SLC7A5 or the SLC7A5/SLC3A2 complex likely interferes with cystine uptake by the SLC3A2/SLC7A11 complex in *trans*.

NAPDH Oxidases Provide One Source of Death-Inducing ROS in Erastin-Treated Cells

Blocking system x_c^- inhibits cysteine-dependent glutathione (GSH) synthesis and also inhibits the transplasma membrane cysteine redox shuttle (Banjac et al., 2008; Ishii et al., 1981). Both effects impair cellular antioxidant defenses, thereby facilitating toxic ROS accumulation. Having ruled out the mitochondrial ETC as a source of death-inducing ROS in erastin-treated cells (Figures 1D–1F), we examined the role of the nicotinamide adenine dinucleotide phosphate (NADPH) oxidase (NOX) family of superoxide-producing enzymes (NOX1–5, DUOX1,2), which are upregulated in several RAS mutant tumors (Kamata, 2009). Erastin-induced ferroptosis was strongly suppressed in Calu-1 cells by the canonical NOX inhibitor diphenylene iodonium (DPI), the NOX1/4-specific inhibitor GKT137831 (Laleu et al., 2010), and an inhibitor of the NADPH-generating pentose phosphate pathway (PPP), 6-aminonicotinamde (6-AN) (Figures 7A and 7B). Given that Calu-1 cells express *NOX1* at much higher levels than *NOX4* (Figure S6A), NOX1 is the most likely candidate to mediate the observed NOX-dependent lethal effects in these cells. Additionally, shRNA-mediated silencing of two PPP enzymes, glucose-6-phosphate dehydrogenase (*G6PD*) and phosphoglycerate dehydrogenase (*PGD*), also prevented erastin-induced ferroptosis in Calu-1 cells to the same extent as silencing of *VDAC2* (Figures 7C and 7D). 6-AN also prevented cell death as well as ROS production in BJeLR cells (Figures S6B and 6C), suggesting an important role for this pathway in these cell types. On the other hand, NOX and PPP inhibitors were only partially effective at preventing erastin-induced ferroptosis in HT-1080 cells (Figure 7B), indicating that other pathways, in addition to the PPP/NOX pathway, can contribute to the onset

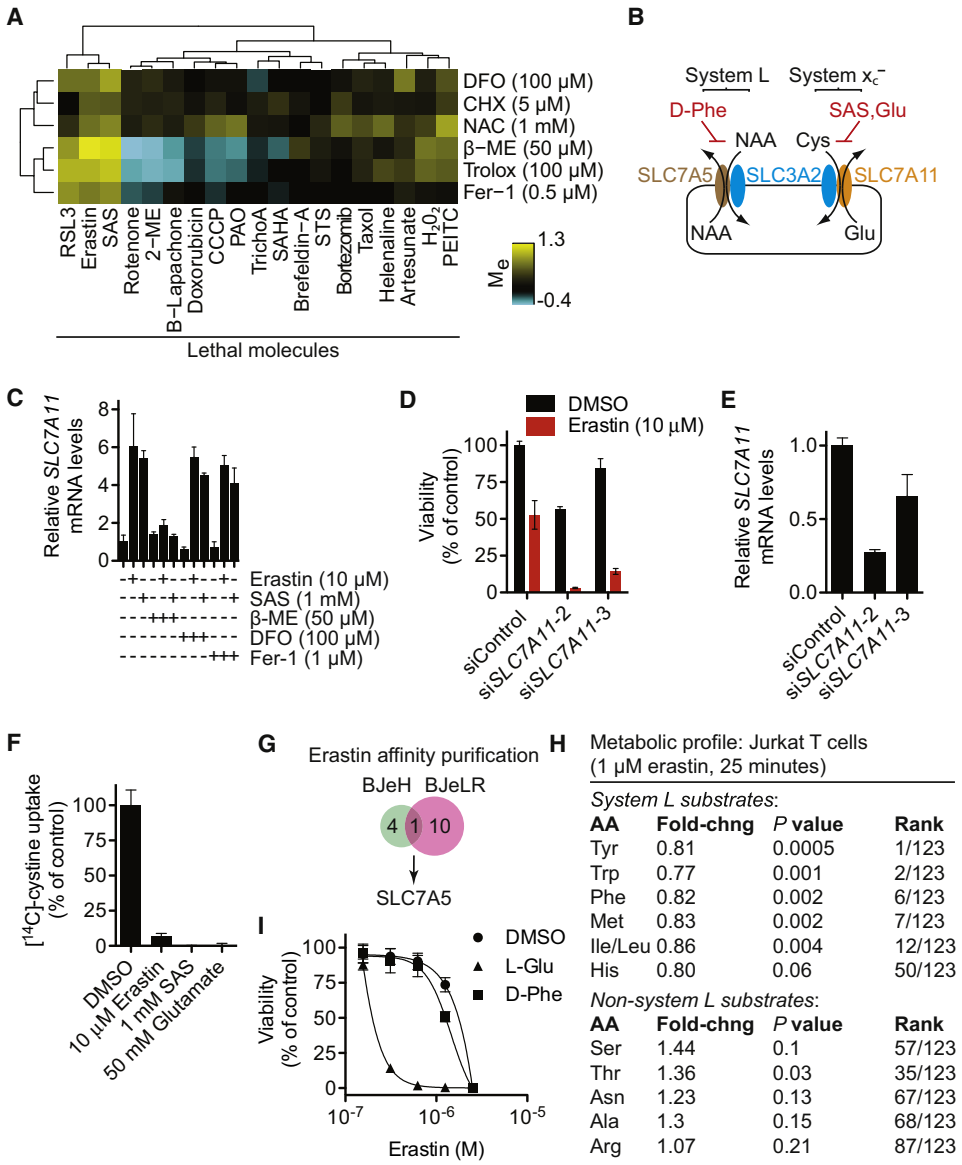

H

Metabolic profile: Jurkat T cells (1 μM erastin, 25 minutes)

System L substrates:

AA	Fold-chng	*P* value	Rank
Tyr	0.81	0.0005	1/123
Trp	0.77	0.001	2/123
Phe	0.82	0.002	6/123
Met	0.83	0.002	7/123
Ile/Leu	0.86	0.004	12/123
His	0.80	0.06	50/123

Non-system L substrates:

AA	Fold-chng	*P* value	Rank
Ser	1.44	0.1	57/123
Thr	1.36	0.03	35/123
Asn	1.23	0.13	67/123
Ala	1.3	0.15	68/123
Arg	1.07	0.21	87/123

Figure 6. Erastin Inhibits the Activity of System x_c^-

(A) Modulatory profile of HT-1080 cells treated with different lethal compounds and inhibitors.

(B) Cartoon depicting the composition and function of system L and system x_c^-. Cys, cystine; NAA, neutral amino acids.

(C) *SLC7A11* mRNA levels in compound-treated (6 hr) HT-1080 cells determined by RT-qPCR.

(D and E) Effect of silencing *SLC7A11* by using siRNA on erastin (10 μM, 8 hr) induced death (D) and mRNA levels (E) in HT-1080 cells.

(F) Normalized Na^+-independent [^{14}C]-cystine uptake by HT-1080 cells in response to various drugs. Data are represented as mean ±SD, n = 3.

(G) Identification of SLC7A5 as the lone target identified by erastin affinity purification in both BJeH and BJeLR cells.

(H) Metabolic profiling of system L and nonsystem L substrate amino acid levels in erastin-treated Jurkat cells.

(I) Effect of L-glutamic acid (L-Glu, 12.5 mM) and D-phenylalanine (D-Phe, 12.5 mM) on erastin-induced death in HT-1080 cells.

See also Figure S5.

of death in erastin-treated cells once the appropriate conditions have been set by the inhibition of system x_c^-.

DISCUSSION

Ferroptotic death is morphologically, biochemically, and genetically distinct from apoptosis, various forms of necrosis, and autophagy. This process is characterized by the overwhelming, iron-dependent accumulation of lethal lipid ROS (Figure 7E, blue outline). Unlike other forms of apoptotic and nonapoptotic death (Christofferson and Yuan, 2010; Jacobson and Raff, 1995), this requirement for ROS accumulation appears to be universal. In at least some cells, NOX family enzymes make important contributions to this process. Indeed, although we

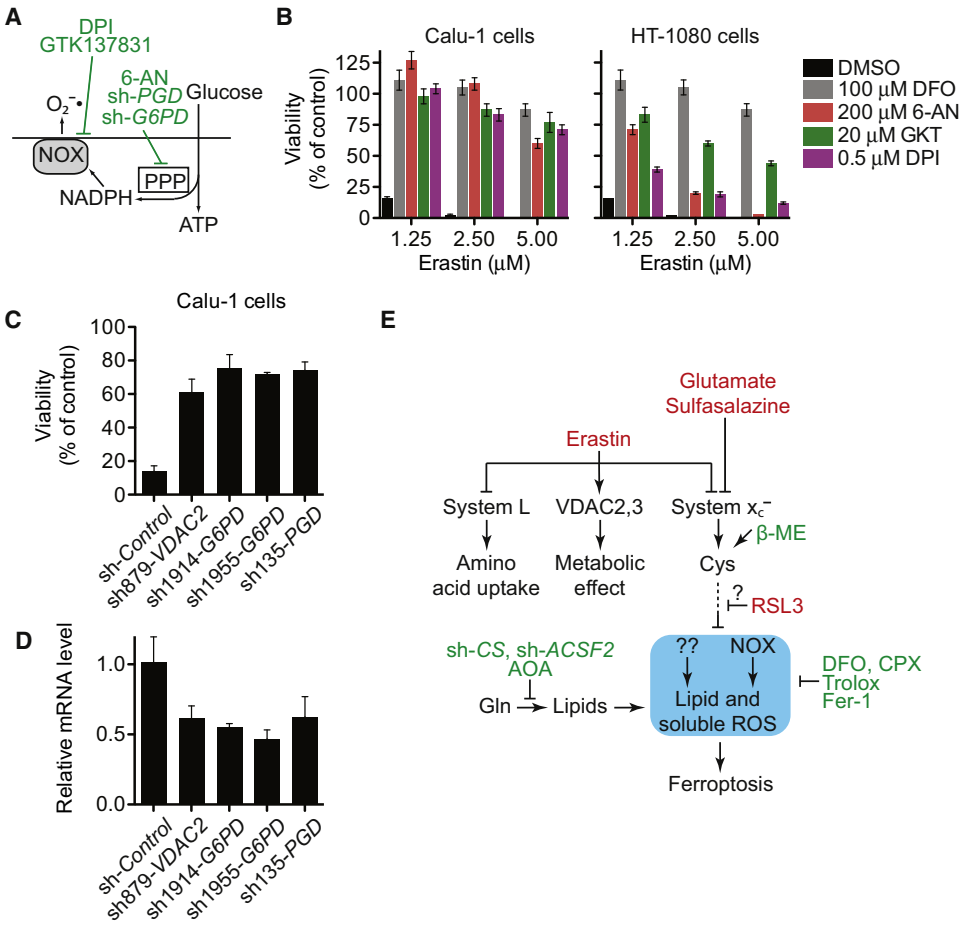

Figure 7. Role of NOX in Erastin-Induced Death

(A) Outline of NOX pathway. Inhibitors are shown in green. PPP, pentose phosphate pathway.

(B) Effect of NOX pathway inhibitors on erastin-induced death in Calu-1 and HT-1080 cells. GKT, GKT137831.

(C and D) Effect of shRNA silencing of the PPP enzymes glucose-6-phosphate dehydrogenase (*G6PD*) and phosphogluconate dehydrogenase (*PGD*) on viability of erastin (2.5 μM)-treated Calu-1 cells. Infection with shRNA targeting *VDAC2* was used as a positive control. Relative mRNA levels in (D) were assessed by RT-qPCR following shRNA knockdown. Data in (B), (C), and (D) represent mean ±SD.

(E) Model of ferroptosis pathway. The core ferroptotic lethal mechanism is highlighted in blue.

See Figure S6 for additional data supporting a role for the PPP/NOX pathway in erastin-induced cell death.

cannot exclude the possibility of a death-inducing protein or protein complex activated downstream of ROS accumulation, we posit that the executioners of death in cancer cells undergoing ferroptosis are these ROS themselves. An important prediction of this model is that, under anoxic conditions, ferroptosis will be inactive. However, even here, agents such as erastin that may prevent uptake of essential amino acids by system L are likely to be toxic to cells.

Using an shRNA library targeting most known genes encoding mitochondrial proteins (Pagliarini et al., 2008), we identified specific roles for *RPL8*, *IREB2*, *ATP5G3*, *TTC35*, *CS*, and *ACSF2* in erastin-induced ferroptosis. A plausible hypothesis to emerge from these data is that *CS* and *ACSF2* are required to synthesize a specific lipid precursor necessary for death (Figure 7E). Just as important, the high resolution of the arrayed approach (1 hairpin/well, minimum 5 hairpins/gene) provides confidence that the various mitochondrial genes not identified in our screen, including many implicated in apoptotic and other nonapoptotic death pathways (*BID*, *BAK1*, *BAX*, *AIFM1*, *PPIF*, *HTRA2*, *ENDOG*, and *PGAM5*), are truly not required for erastin-induced ferroptosis. This screening collection will be a valuable resource for future studies of the role of the mitochondria in cell physiology.

In cancer cells, inhibition of system x_c^--mediated cystine uptake by erastin, SAS, or glutamate may be sufficient to initiate iron-dependent ferroptosis. Inhibition of system x_c^- is, however, not necessary; RSL3 does not inhibit cystine uptake and yet triggers an otherwise similar iron- and ROS-dependent ferroptototic death program. Thus, RSL3 likely modulates the activity of a target lying downstream of or in parallel to system x_c^- (Figure 7E). Importantly, this may enable RSL3 to activate ferroptosis in cells or conditions in which cystine uptake via system x_c^- is not limiting for survival. Lanperisone, another recently identified oncogenic RAS-selective lethal small molecule that causes

nonapoptotic, iron-dependent death in mouse *Kras* mutant tumor cells (Shaw et al., 2011), may also inhibit the function of system x_c^- or another target in the ferroptotic pathway. Other compounds that behave as RSLs, such as PEITC, oncrasin, and piperlongumine (Guo et al., 2008; Raj et al., 2011; Trachootham et al., 2006), trigger mitochondrial cytochrome *c* release, caspase activation, and other features of apoptosis not observed in cancer cells undergoing ferroptosis. Certain tumor cells are highly resistant to apoptosis (Ni Chonghaile et al., 2011). Thus, agents such as erastin, RSL3, and lanperisone that can trigger nonapoptotic death may exhibit a unique spectrum of clinical activity.

In some brain cell populations, inhibition of system x_c^- by glutamate triggers oxidative cell death dependent on iron and lipid ROS as well as Ca^{2+} influx, mitochondrial damage, mitochondrial ROS production, and chromatin fragmentation (Li et al., 1997; Murphy et al., 1989; Ratan et al., 1994; Tan et al., 1998; Yonezawa et al., 1996). These latter events, beginning with Ca^{2+} influx, are not required for RSL-induced ferroptosis in cancer cells, perhaps because heightened activity of NOX or other pro-oxidant enzymes or basally altered membrane lipid composition is sufficient to promote death in the absence of these additional features. Regardless, the oxidative death pathways triggered in cancer cells and brain cells by blockade of cystine uptake both appear to access a core iron- and ROS-dependent ferroptotic mechanism, accounting for the ability of Fer-1 and CPX to attenuate death in both cases (Figure 7E).

The specific role of iron in ferroptosis remains unclear. Ferroptosis cannot be explained by a simple increase in H_2O_2-dependent, iron-catalyzed ROS production (i.e., Fenton chemistry), as H_2O_2-induced death is distinct from RSL-induced ferroptosis (Figures 1 and 2). Rather, our results are most consistent with one or more iron-dependent enzymes functioning as part of the core oxidative lethal mechanism. The void created in the antioxidant defenses of the cell by the inhibition of cystine uptake by erastin may be required to unleash the activity of these enzymes. Thus, for better or worse, the aberrantly elevated levels of iron that are observed in some cancer cells (Pinnix et al., 2010) and pathological neuronal populations (Duce et al., 2010; Lei et al., 2012) may predispose to ferroptotic death in situations of cystine or cysteine limitation.

EXPERIMENTAL PROCEDURES

Analysis of Reactive Oxygen Species Production

The day before the experiment, 200,000 cells/well were seeded in 6-well dishes (Corning). The day of the experiment, cells were treated with test compounds for the indicated times; harvested by trypsinizaiton; resuspended in 500 μl Hanks Balanced Salt Solution (HBSS, Gibco) containing H_2DCFDA (25 μM), C11-BODIPY(581/591) (2 μM), or MitoSOX (5 μM) (all from Molecular Probes, Invitrogen); and incubated for 10 min at 37°C in a tissue culture incubator. Cells were then resuspended in 500 μl of fresh HBSS, strained through a 40 μM cell strainer (BD Falcon), and analyzed using a flow cytometer (FACSCalibur or Accuri C6, BD Biosciences) equipped with 488 nm laser for excitation. Data were collected from the FL1 (H_2DCFDA, C11-BODIPY) or FL2 channel (MitoSOX). A minimum of 10,000 cells were analyzed per condition.

Cancer Cell Viability Measurements

Cell viability was typically assessed in 384-well format by Alamar Blue (Invitrogen) fluorescence (ex/em 530/590) measured on a Victor3 plate reader (Perkin Elmer). In some experiments, Trypan blue dye exclusion counting was performed by using an automated cell counter (ViCell, Beckman-Coulter). Cell viability under test conditions is reported as a percentage relative to the negative control treatment.

shRNA Screening

An arrayed collection of 6,528 shRNA hairpins derived from The RNAi Consortium (TRC) collection targeting 1,087 genes, kindly provided by Vamsi Mootha and Joshua Baughman (MIT), was screened in 384-well plate format (Corning) in both Calu-1 and HT-1080 cells. shRNAs targeting *GFP* and *RFP*, randomly distributed through each plate, served as negative controls. Four-hundred cells/well were infected in duplicate for 48 hr with 2 μl shRNA-containing viral supernatant, selected for 24 hr in puromycin (1.5 μg/ml), and then treated with DMSO, erastin (7.3 μM), or STS (1 μM) for 24 hr. Cell viability was determined by using Alamar Blue. For each hairpin within each treatment condition, a cell death rescue score was computed as the ratio of the average viability of the two replicates to the average viability of the within-plate negative controls. These scores were used to compare the effects between compounds. To identify genes required for ferroptosis, individual hairpins were scored as hits if they displayed an average death suppression $\geq$3 median average deviations from the median within-plate or screen-wide negative control values. Fifty-one candidate genes were identified with the same two (or more) unique hairpins per gene called as hits in both the Calu-1 and HT-1080 screens. For each candidate gene, confirmation studies using reverse-transcription quantitative PCR (RT-qPCR) analysis of mRNA silencing were performed in HT-1080 cells by using freshly prepared virus as described in greater detail in the Extended Experimental Procedures.

[^{14}C]-Cystine Uptake Assay

Two-hundred thousand (200,000) HT-1080 cells/well were seeded overnight in 6-well dishes (Corning). The next day, cells were washed twice in prewarmed Na^+-free uptake buffer (137 mM choline chloride, 3 mM KCl, 1 mM $CaCl_2$, 1 mM $MgCl_2$, 5 mM D-glucose, 0.7 mM K_2HPO_4, and 10 mM HEPES [pH 7.4]) and then incubated for 10 min at 37°C in 1 ml of uptake buffer to deplete cellular amino acids. At this point, in each well, the buffer was replaced with 600 μl uptake buffer containing compound and 0.12 μCi (80–110 mCi/mmol) of L-[3,3′-^{14}C]-cystine (Perkin Elmer) and incubated for 3 min at 37°C. Cells were then washed three times with ice-cold uptake buffer and lysed in 500 μl 0.1 M NaOH. To this lysate, 15 ml of scintillation fluid was added, and radioactive counts per minute were obtained by using a scintillation counter. All measurements were performed in triplicate for each condition.

Statistical Analyses

All statistical analyses were performed by using Prism 5.0c (GraphPad Software).

SUPPLEMENTAL INFORMATION

Supplemental Information includes Extended Experimental Procedures and six figures and can be found with this article online at doi:10.1016/j.cell.2012.03.042.

ACKNOWLEDGMENTS

We thank Vamsi Mootha, Joshua Baughman, and David Root for sharing the custom shRNA library; Kristy Brown and Elma Zaganjor for assistance with electron microscopy; Darnelle Delva for help with qPCR; Rohitha SriRamaratnam for help with cell death assays; Eric Schon for providing the 143B cell lines; Craig Thompson for providing *Bax*$^{-/-}$ *Bak*$^{-/-}$ MEFs; and Patrick Page (GenKyoTex S.A.) for providing GKT137831. We thank David Clarke for comments on the manuscript. Certain shRNA collections used in this work were generated with the assistance of the Scientific Planning and Allocation of Resources Committee (SPARC, to Vamsi Mootha). NSF grant CHE-0840451 supported the purchase and operation of equipment used in the chemical characterization of ferrostatin-1. M.R.L. was supported by a fellowship from the National Science Foundation. K.M.L. was supported

by the Medical Scientist Training Program (Columbia University). S.J.D. was supported by a postdoctoral fellowship from the Canadian Institutes of Health Research. This research was supported by grants from the US National Institutes of Health (5R01CA097061, 5R01GM085081, and R01CA161061), the Arnold and Mabel Beckman Foundation, and NYSTAR. B.R.S. is an Early Career Scientist of the Howard Hughes Medical Institute.

Received: January 17, 2012
Revised: March 9, 2012
Accepted: March 13, 2012
Published: May 24, 2012

REFERENCES

Banjac, A., Perisic, T., Sato, H., Seiler, A., Bannai, S., Weiss, N., Kölle, P., Tschoep, K., Issels, R.D., Daniel, P.T., et al. (2008). The cystine/cysteine cycle: a redox cycle regulating susceptibility versus resistance to cell death. Oncogene *27*, 1618–1628.

Bergsbaken, T., Fink, S.L., and Cookson, B.T. (2009). Pyroptosis: host cell death and inflammation. Nat. Rev. Microbiol. *7*, 99–109.

Cater, H.L., Gitterman, D., Davis, S.M., Benham, C.D., Morrison, B., III, and Sundstrom, L.E. (2007). Stretch-induced injury in organotypic hippocampal slice cultures reproduces in vivo post-traumatic neurodegeneration: role of glutamate receptors and voltage-dependent calcium channels. J. Neurochem. *101*, 434–447.

Cheah, J.H., Kim, S.F., Hester, L.D., Clancy, K.W., Patterson, S.E., III, Papadopoulos, V., and Snyder, S.H. (2006). NMDA receptor-nitric oxide transmission mediates neuronal iron homeostasis via the GTPase Dexras1. Neuron *51*, 431–440.

Choi, D.W. (1988). Glutamate neurotoxicity and diseases of the nervous system. Neuron *1*, 623–634.

Christofferson, D.E., and Yuan, J. (2010). Necroptosis as an alternative form of programmed cell death. Curr. Opin. Cell Biol. *22*, 263–268.

Dolma, S., Lessnick, S.L., Hahn, W.C., and Stockwell, B.R. (2003). Identification of genotype-selective antitumor agents using synthetic lethal chemical screening in engineered human tumor cells. Cancer Cell *3*, 285–296.

Duce, J.A., Tsatsanis, A., Cater, M.A., James, S.A., Robb, E., Wikhe, K., Leong, S.L., Perez, K., Johanssen, T., Greenough, M.A., et al. (2010). Iron-export ferroxidase activity of β-amyloid precursor protein is inhibited by zinc in Alzheimer's disease. Cell *142*, 857–867.

Fuchs, Y., and Steller, H. (2011). Programmed cell death in animal development and disease. Cell *147*, 742–758.

Gout, P.W., Buckley, A.R., Simms, C.R., and Bruchovsky, N. (2001). Sulfasalazine, a potent suppressor of lymphoma growth by inhibition of the x(c)- cystine transporter: a new action for an old drug. Leukemia *15*, 1633–1640.

Guo, W., Wu, S., Liu, J., and Fang, B. (2008). Identification of a small molecule with synthetic lethality for K-ras and protein kinase C iota. Cancer Res. *68*, 7403–7408.

Ishii, T., Bannai, S., and Sugita, Y. (1981). Mechanism of growth stimulation of L1210 cells by 2-mercaptoethanol in vitro. Role of the mixed disulfide of 2-mercaptoethanol and cysteine. J. Biol. Chem. *256*, 12387–12392.

Jacobson, M.D., and Raff, M.C. (1995). Programmed cell death and Bcl-2 protection in very low oxygen. Nature *374*, 814–816.

Kamata, T. (2009). Roles of Nox1 and other Nox isoforms in cancer development. Cancer Sci. *100*, 1382–1388.

Kanai, Y., and Endou, H. (2003). Functional properties of multispecific amino acid transporters and their implications to transporter-mediated toxicity. J. Toxicol. Sci. *28*, 1–17.

Laleu, B., Gaggini, F., Orchard, M., Fioraso-Cartier, L., Cagnon, L., Houngninou-Molango, S., Gradia, A., Duboux, G., Merlot, C., Heitz, F., et al. (2010). First in class, potent, and orally bioavailable NADPH oxidase isoform 4 (Nox4) inhibitors for the treatment of idiopathic pulmonary fibrosis. J. Med. Chem. *53*, 7715–7730.

Lei, P., Ayton, S., Finkelstein, D.I., Spoerri, L., Ciccotosto, G.D., Wright, D.K., Wong, B.X., Adlard, P.A., Cherny, R.A., Lam, L.Q., et al. (2012). Tau deficiency induces parkinsonism with dementia by impairing APP-mediated iron export. Nat. Med. *18*, 291–295.

Li, Y., Maher, P., and Schubert, D. (1997). A role for 12-lipoxygenase in nerve cell death caused by glutathione depletion. Neuron *19*, 453–463.

Lo, M., Ling, V., Wang, Y.Z., and Gout, P.W. (2008). The xc- cystine/glutamate antiporter: a mediator of pancreatic cancer growth with a role in drug resistance. Br. J. Cancer *99*, 464–472.

Lossi, L., Alasia, S., Salio, C., and Merighi, A. (2009). Cell death and proliferation in acute slices and organotypic cultures of mammalian CNS. Prog. Neurobiol. *88*, 221–245.

Macarron, R., Banks, M.N., Bojanic, D., Burns, D.J., Cirovic, D.A., Garyantes, T., Green, D.V., Hertzberg, R.P., Janzen, W.P., Paslay, J.W., et al. (2011). Impact of high-throughput screening in biomedical research. Nat. Rev. Drug Discov. *10*, 188–195.

Morrison, B., III, Pringle, A.K., McManus, T., Ellard, J., Bradley, M., Signorelli, F., Iannotti, F., and Sundstrom, L.E. (2002). L-arginyl-3,4-spermidine is neuroprotective in several in vitro models of neurodegeneration and in vivo ischaemia without suppressing synaptic transmission. Br. J. Pharmacol. *137*, 1255–1268.

Mullen, A.R., Wheaton, W.W., Jin, E.S., Chen, P.H., Sullivan, L.B., Cheng, T., Yang, Y., Linehan, W.M., Chandel, N.S., and Deberardinis, R.J. (2011). Reductive carboxylation supports growth in tumour cells with defective mitochondria. Nature *481*, 385–388.

Murphy, T.H., Miyamoto, M., Sastre, A., Schnaar, R.L., and Coyle, J.T. (1989). Glutamate toxicity in a neuronal cell line involves inhibition of cystine transport leading to oxidative stress. Neuron *2*, 1547–1558.

Ni Chonghaile, T., Sarosiek, K.A., Vo, T.T., Ryan, J.A., Tammareddi, A., Moore, Vdel.G., Deng, J., Anderson, K.C., Richardson, P., Tai, Y.T., et al. (2011). Pretreatment mitochondrial priming correlates with clinical response to cytotoxic chemotherapy. Science *334*, 1129–1133.

Noraberg, J., Poulsen, F.R., Blaabjerg, M., Kristensen, B.W., Bonde, C., Montero, M., Meyer, M., Gramsbergen, J.B., and Zimmer, J. (2005). Organotypic hippocampal slice cultures for studies of brain damage, neuroprotection and neurorepair. Curr. Drug Targets CNS Neurol. Disord. *4*, 435–452.

Pagliarini, D.J., Calvo, S.E., Chang, B., Sheth, S.A., Vafai, S.B., Ong, S.E., Walford, G.A., Sugiana, C., Boneh, A., Chen, W.K., et al. (2008). A mitochondrial protein compendium elucidates complex I disease biology. Cell *134*, 112–123.

Pinnix, Z.K., Miller, L.D., Wang, W., D'Agostino, R., Jr., Kute, T., Willingham, M.C., Hatcher, H., Tesfay, L., Sui, G., Di, X., et al. (2010). Ferroportin and iron regulation in breast cancer progression and prognosis. Sci. Transl. Med. *2*, 43ra56.

Raj, L., Ide, T., Gurkar, A.U., Foley, M., Schenone, M., Li, X., Tolliday, N.J., Golub, T.R., Carr, S.A., Shamji, A.F., et al. (2011). Selective killing of cancer cells by a small molecule targeting the stress response to ROS. Nature *475*, 231–234.

Ramanathan, A., and Schreiber, S.L. (2009). Direct control of mitochondrial function by mTOR. Proc. Natl. Acad. Sci. USA *106*, 22229–22232.

Ratan, R.R., Murphy, T.H., and Baraban, J.M. (1994). Oxidative stress induces apoptosis in embryonic cortical neurons. J. Neurochem. *62*, 376–379.

Salahudeen, A.A., Thompson, J.W., Ruiz, J.C., Ma, H.W., Kinch, L.N., Li, Q., Grishin, N.V., and Bruick, R.K. (2009). An E3 ligase possessing an iron-responsive hemerythrin domain is a regulator of iron homeostasis. Science *326*, 722–726.

Sato, H., Tamba, M., Ishii, T., and Bannai, S. (1999). Cloning and expression of a plasma membrane cystine/glutamate exchange transporter composed of two distinct proteins. J. Biol. Chem. *274*, 11455–11458.

Shaw, A.T., Winslow, M.M., Magendantz, M., Ouyang, C., Dowdle, J., Subramanian, A., Lewis, T.A., Maglathin, R.L., Tolliday, N., and Jacks, T. (2011). Selective killing of K-ras mutant cancer cells by small molecule inducers of oxidative stress. Proc. Natl. Acad. Sci. USA *108*, 8773–8778.

Sundstrom, L., Morrison, B., III, Bradley, M., and Pringle, A. (2005). Organotypic cultures as tools for functional screening in the CNS. Drug Discov. Today *10*, 993–1000.

Tan, S., Sagara, Y., Liu, Y., Maher, P., and Schubert, D. (1998). The regulation of reactive oxygen species production during programmed cell death. J. Cell Biol. *141*, 1423–1432.

Thompson, C.B. (1995). Apoptosis in the pathogenesis and treatment of disease. Science *267*, 1456–1462.

Trachootham, D., Zhou, Y., Zhang, H., Demizu, Y., Chen, Z., Pelicano, H., Chiao, P.J., Achanta, G., Arlinghaus, R.B., Liu, J., and Huang, P. (2006). Selective killing of oncogenically transformed cells through a ROS-mediated mechanism by beta-phenylethyl isothiocyanate. Cancer Cell *10*, 241–252.

Vashisht, A.A., Zumbrennen, K.B., Huang, X., Powers, D.N., Durazo, A., Sun, D., Bhaskaran, N., Persson, A., Uhlen, M., Sangfelt, O., et al. (2009). Control of iron homeostasis by an iron-regulated ubiquitin ligase. Science *326*, 718–721.

Vigil, D., Cherfils, J., Rossman, K.L., and Der, C.J. (2010). Ras superfamily GEFs and GAPs: validated and tractable targets for cancer therapy? Nat. Rev. Cancer *10*, 842–857.

Wang, Y., Dawson, V.L., and Dawson, T.M. (2009). Poly(ADP-ribose) signals to mitochondrial AIF: a key event in parthanatos. Exp. Neurol. *218*, 193–202.

Watkins, P.A., Maiguel, D., Jia, Z., and Pevsner, J. (2007). Evidence for 26 distinct acyl-coenzyme A synthetase genes in the human genome. J. Lipid Res. *48*, 2736–2750.

Wise, D.R., DeBerardinis, R.J., Mancuso, A., Sayed, N., Zhang, X.Y., Pfeiffer, H.K., Nissim, I., Daikhin, E., Yudkoff, M., McMahon, S.B., and Thompson, C.B. (2008). Myc regulates a transcriptional program that stimulates mitochondrial glutaminolysis and leads to glutamine addiction. Proc. Natl. Acad. Sci. USA *105*, 18782–18787.

Wolpaw, A.J., Shimada, K., Skouta, R., Welsch, M.E., Akavia, U.D., Pe'er, D., Shaik, F., Bulinski, J.C., and Stockwell, B.R. (2011). Modulatory profiling identifies mechanisms of small molecule-induced cell death. Proc. Natl. Acad. Sci. USA *108*, E771–E780.

Yagoda, N., von Rechenberg, M., Zaganjor, E., Bauer, A.J., Yang, W.S., Fridman, D.J., Wolpaw, A.J., Smukste, I., Peltier, J.M., Boniface, J.J., et al. (2007). RAS-RAF-MEK-dependent oxidative cell death involving voltage-dependent anion channels. Nature *447*, 864–868.

Yang, W.S., and Stockwell, B.R. (2008). Synthetic lethal screening identifies compounds activating iron-dependent, nonapoptotic cell death in oncogenic-RAS-harboring cancer cells. Chem. Biol. *15*, 234–245.

Yonezawa, M., Back, S.A., Gan, X., Rosenberg, P.A., and Volpe, J.J. (1996). Cystine deprivation induces oligodendroglial death: rescue by free radical scavengers and by a diffusible glial factor. J. Neurochem. *67*, 566–573.